Fabrication of a Plasma Electrolytic Oxidation/Anodic Aluminum Oxide Multi-Layer Film via One-Step Anodizing Aluminum in Ammonium Carbonate

Tatsuya Kikuchi[1,*], Taiki Taniguchi[1], Ryosuke O. Suzuki[1], Shungo Natsui[2]

[1]Faculty of Engineering, Hokkaido University, N13-W8, Kita-ku, Sapporo, Hokkaido, 060-8628, Japan
[2]Institute of Multidisciplinary Research for Advanced Materials, Tohoku University, Katahira 2-1-1, Aoba-ku, Sendai, 980-8577, Japan

*Corresponding author: Tatsuya Kikuchi
e-mail: kiku@eng.hokudai.ac.jp

Abstract

A plasma electrolytic oxidation (PEO)/anodic aluminum oxide (AAO) multi-layer film was fabricated via one-step galvanostatic anodizing of high-purity aluminum in 0.3-2.0 M ammonium carbonate ($(NH_4)_2CO_3$) solutions at 283-333 K and 25-400 Am^{-2}. Anodizing at higher concentrations and higher temperatures caused the formation of relatively uniform anodic oxide film on the aluminum substrate. Characteristic voltage-time curves with two high-plateau voltages at approximately 250 V and 375 V were obtained during galvanostatic anodizing. A multi-layer structure of an outer PEO layer with a crystalline γ-Al_2O_3 structure and an inner amorphous AAO layer with nano-cylinerical pores was formed by continuous visible sparking occurring after passing the first voltage plateau region. The whole aluminum surface was covered with the multi-layer structure after reaching the second voltage region. The thickness of the multi-layer increased with time via the further anodizing process at the second plateau voltage. Pore sealing of the inner nanoporous film was achieved by immersion post-treatment in boiling water.

Keywords: Anodizing; Aluminum; Ammonium Carbonate; Plasma Electrolytic Oxidation; Anodic Aluminum Oxide

1. Introduction

Electrochemical anodizing (also known as anodization) is one of the most important surface finishing techniques for the passivation, hardening, and functionalization of aluminum and its alloys. Characteristic anodic oxide films with different micro- and nano-morphologies can be fabricated by the variations in anodizing conditions, such as electrochemical parameters and electrolyte species used [1-3]. Anodizing aluminum in neutral electrolyte solutions, such as borate (H_3BO_3/$Na_2B_4O_7$) and ammonium tartrate ($(NH_4)_2C_4H_4O_6$), leads to the surface coating of a compact, thin barrier oxide film [4-8]. This barrier film consists of an amorphous aluminum oxide containing electrolyte anions and is widely investigated and applied for aluminum electrolytic capacitor applications due to their high dielectric property. On the other hand, anodizing aluminum in acidic or alkaline electrolyte solutions, such as sulfuric acid (H_2SO_4), selenic acid (H_2SeO_4), oxalic acid $(COOH)_2$, phosphonic acid (H_3PO_4), phosphoric acid (H_3PO_3), etidronic acid ($CH_3C(OH)[PO(OH)_2]_2$), and sodium tetraborate ($Na_2B_4O_7$), leads to the surface coating of a thick, porous oxide film with vertical nanoscale pores (typically known as anodic aluminum oxide, AAO, or porous anodic alumina) [9-15]. Numerous nanopores formed in this AAO film can easily be filled with pseudoboehmite by the subsequent pore-sealing process [16,17]. Therefore, the AAO film is widely used to improve the corrosion-resistant property of various aluminum alloys [18-20]. In addition, the AAO film possesses a characteristic honeycomb nanostructure with self-organized nanopores and thus has been widely used to fabricate various nanomaterials via the high-aspect ratio nanoporous structure [21-26].

Anodizing aluminum at extremely higher voltages measuring more than 200-300 V leads to the continuous visible sparking behaviors caused by microdischarge plasma, and a hard oxide film is formed on the whole surface of the aluminum anode (known as plasma electrolytic oxidation, PEO, or microarc oxidation) [27]. This PEO film can be typically formed via anodizing aluminum in several alkaline solutions such as sodium hydroxide (NaOH), potassium hydroxide (KOH), sodium metasilicate (Na_2SiO_3), sodium tungstate (Na_2WO_4), sodium tetraborate, and mixtures of these solutions [28-36]. The PEO film consists of a crystalline α- or γ-aluminum oxide with a microporous structure measuring several tens of micrometers in thickness, and the Vickers hardness of the PEO film is larger than that of the AAO film formed by hard anodizing at low temperature [37,38]. Therefore, the PEO coating enhances the wear resistance, mechanical hardness, and corrosion resistance of the aluminum and its alloys, and was recently investigated for various mechanical components such as motor vehicles and industrial machines. As mentioned above, both the AAO and PEO coating processes are important surface finishing methods for aluminum and its alloys.

In the present investigation, we demonstrated the fabrication of a PEO/AAO multi-layer anodic oxide film via one-step anodizing of aluminum in an alkaline electrolyte solution, ammonium carbonate ($(NH_4)_2CO_3$). The growth behavior and

nanostructural features of the anodic coatings formed in ammonium carbonate solutions were examined by electrochemical measurements and electron microscopy. A characteristic multi-layer structure consisting of an outer PEO film and an inner AAO film can be fabricated via simple anodizing in ammonium carbonate solution by choosing the appropriate operating condition.

2. Experimental

Aluminum plates of 99.999 wt% high purity (width: 10 mm, height: 20 mm, and thickness: 250 μm; the plates had an electric connecting handle and were manufactured by Nippon Light Metal, Japan) were used as anodizing materials. The aluminum specimens were immersed in 99.5 % ethanol at room temperature and were ultrasonically cleaned for 10 min. After cleaning, the bottom half of the electric connecting handle was covered with an insulation silicone resin (KE45W, Shin-Etsu, Japan). Next, the specimens were immersed in a 78 vol% CH_3COOH/22 vol% 70%-$HClO_4$ solution at 280 K and were anodically polarized at a constant voltage of 28 V for 1 min to electropolish the aluminum surface. A large aluminum plate (99.99 wt%; Nippon Light Metal, Japan) was used as the cathode, and the electrolyte solution was slowly stirred with a magnetic stirrer during electropolishing. After electropolishing, the specimens were washed immediately with ultrapure water and then were dried.

The electropolished aluminum specimens were anodized in ammonium carbonate solution under various operating conditions. An electrochemical glass cell (inner diameter: 55 mm) with a 0.3- to 2.0-M ammonium carbonate solution (solution volume: 150 mL; Kanto Chemical, Japan) was maintained in a constant-temperature water bath (UCT-1000, AS ONE, Japan). The aluminum anode and platinum cathode (99.95 wt%, thickness: 200 μm, Nilaco, Japan) were immersed in the electrolyte solution at 283-333 K and were galvanostatically anodized at 25-400 Am^{-2} for up to 670 min with a direct power supply (PWR400H; Kikusui Electronics, Japan). The electrolyte solution was stirred at a rotating speed of 250 rpm with a magnetic stirrer (MIXcontrol 40 and MIXdrive 1 XS; 2mag AG, Germany). The anodizing voltage during galvanostatic anodizing was measured using a PC-connected digital multimeter (DMM4040; Tektronix, USA). After anodizing, the specimens were washed immediately with ultrapure water and then were dried. The anodized specimens were immersed in boiling ultrapure water to seal the pores formed in the AAO film.

The surface, fractured cross section, and vertical cross section of the anodized specimens were examined by scanning electron microscopy (SEM; TM-1000, Hitachi High-Technologies, Japan, 15 kV) (JSM6500F; JEOL, Japan, 10 kV). A thin electroconductive platinum layer was formed on the surface of the anodized specimens before SEM observations. For the observations of vertical cross sections, the anodized specimens were embedded in an epoxy resin, were mechanically polished with SiC papers, and finally were buffed with a diamond paste (grain size: 1 μm). Several polished specimens were chemically etched in a 4.17 M NaOH/0.25 M $K_3[Fe(CN)_6]$

solution for 20 s. The thickness of the anodic oxide was measured from the SEM images using image analysis software (Image-Pro 10, Media Cybernetics, USA). The phase composition of the anodic oxides was identified by thin-film X-ray diffraction analysis (XpertPro, Phillips, Netherlands) using Cu-Kα radiation.

3. Results and Discussion

Figure 1 shows the changes in the voltage, U_a, with the anodizing time, t_a, during galvanostatic anodizing at 25-200 Am^{-2} in a 0.3 M ammonium carbonate solution (333 K). At the lowest current density of 25 Am^{-2}, the voltage was linearly increased to approximately 300 V during the initial stage for 10 min. Although the slope of this voltage-time curve decreased in the period for 10-20 min, the voltage continuously increased to approximately 380 V with the anodizing time. Finally, the voltage maintained a plateau value of approximately 380 V with small unstable oscillations during the remaining anodizing time. Similar voltage-time curves consisting of the initial voltage increase and subsequent plateau voltage with unstable oscillations were obtained at the higher current densities of 50-200 Am^{-2}. Because the edges of the aluminum substrate were electrochemically dissolved during anodizing at the high current densities of 100 Am^{-2} and 200 Am^{-2}, the voltages decrease significantly for 10-20 min. An inset photo shows the surface appearance of the aluminum specimen anodized at 50 Am^{-2} for 120 min. A considerably uneven surface with a nonuniform dark gray oxide film formed in the upper right region, and a lustrous aluminum exposed in the lower left region can be observed here. Such nonuniform coatings were also achieved at other current densities of 25-200 Am^{-2}. Thus, these anodizing conditions are unsuitable for the formation of uniform anodic oxide films.

Figure 2 shows the voltage-time curves obtained by galvanostatic anodizing in a higher concentration of 2.0 M at a) 283 K, b) 303 K, and c) 333 K. During each galvanostatic anodizing at different temperatures, similar voltage changes were measured as follows: the voltages rapidly increased during the initial stage of anodizing, showed a plateau value of approximately 250 V, increased once again, and finally reached a plateau value of approximately 350-380 V. This characteristic voltage-time curves consisting of two-step voltage increase will be discussed later by nanostructural characterization. Visible sparking and gas evolution were continuously observed on the aluminum surface during galvanostatic anodizing after the first plateau voltage of 250 V. Excess current density at higher concentrations caused the sudden decrease in the voltage after reaching more than the second plateau value of voltage due to active dissolution of the aluminum substrate (Fig. 2b, 400 Am^{-2} and Fig. 2c, 100-400 Am^{-2}). Comparing the surface appearances obtained in the different concentrations (inset photos shown in Figs. 2a through 2c), the whole aluminum surface was covered with a matte-finished anodic oxide in all cases. However, the uniformity of the anodic oxide increased with the solution temperature, and a uniform oxide film with a light gray hue was formed at 333 K (Fig. 2c). Therefore, the micro- and nanostructural features of the

specimen anodized at 333 K were examined by SEM.

Figure 3 summarizes a voltage-time curve obtained by long-term anodizing in a 2.0 M ammonium carbonate solution (333 K) at 25 Am^{-2} for 300 min and the corresponding SEM images of the surface and vertical cross-section of the specimens obtained at different anodizing stages. Here, the lowest current density of 25 Am^{-2} was selected to examine in detail the nanostructural changes of the anodic oxide during anodizing, and these SEM images were obtained by anodizing for each operating time. As described in Fig. 2, two clear plateau voltages measuring approximately 250 V for 10-80 min and subsequently 375 V after 180 min were revealed in the voltage-time curve (Fig. 3a). When the aluminum specimen was anodized for 3 min, the voltage rapidly increased with the anodizing time, and a flat, uniform barrier oxide film without any defects was formed on the aluminum surface (Figs. 3b and 3c). As the anodizing time increased to 10 min (first plateau voltage at 250 V), visible sparking was continuously observed on the aluminum specimen, and uneven circular defects and numerous cracks originating from the sparking were observed on the barrier oxide film. These defects were gradually expanded to the whole surface with the anodizing time, and the aluminum surface was completely covered with a rough anodic oxide possessing numerous concaves for 100 min. The vertical cross section at this stage shows nonuniform oxide film consisting of an outer microporous layer and an inner compact layer on the aluminum surface. The roughness of the anodic oxide gradually increased with the anodizing time, and an extremely rough oxide film possessing large-scale crevasses was observed via anodizing for 180 min and 300 min. A high-magnification SEM image of the rough surface formed by anodizing for 180 min is shown in Fig. 3d, and typical morphology of the PEO film with a microporous structure can be observed on the surface. Based on these SEM observations, the anodic oxide grew through the following stages: a) formation of a thin barrier layer, b) formation of a microporous structure, and c) thickening and roughness increase in the microporous structure.

The average thickness of the anodic oxide formed for each anodizing time was quantified using the cross-sectional image and image analysis software, and the changes in the thickness of the oxide film, δ, with the anodizing time, t_a, obtained by anodizing at 25 Am^{-2} and 50 Am^{-2} are shown in Figure 4. At i_a = 25 Am^{-2}, the thickness of the oxide film increased with the anodizing time, although the growth rate gradually decreased with the time. As the current density increased to 50 Am^{-2}, the thickness of the oxide film also increased. However, there was no proportional relationship between the thickness and current density, and the thickness slightly increased to approximately 20-30 % as the current density became two-fold. Such disappearance may be due to the side reaction of oxygen gas evolution from the aluminum anode during galvanostatic anodizing.

The structural features of the microporous anodic oxide will now be discussed in detail. Figure 5a shows an SEM image of the vertical cross section of the specimen

anodized at 25 Am^{-2} in 2.0 M ammonium carbonate solution (333 K) for 670 min. The anodic oxide consisting of an outer microporous layer and an inner compact layer was observed on the aluminum surface; such a multi-layer structure can be observed in the cross sections formed by anodizing for more than 80 min, as shown in Fig. 3. Because this cross-sectional specimen was mechanically polished with SiC paper and buffed with a diamond paste before observation, it was difficult to observe clearly the nanostructure of the anodic oxide. Therefore, the cross-sectional specimen was chemically etched in a $NaOH/K_3[Fe(CN)_6]$ solution for a short time [39], and an SEM image of the etched specimen is shown in Fig. 5b. Note that many nanoscale pores vertically formed to the aluminum substrate can be observed in the inner oxide layer, although no morphological change was observed in the outer microporous layer. To clearly observe the nanostructure of the multi-layer anodic oxide formed by anodizing, fractured cross sections of the anodized specimens were examined by high-magnification SEM.

Figure 6a shows an SEM image of the surface of the specimen anodized at 25 Am^{-2} in a 2.0 M ammonium carbonate solution (333 K) for 10 min, and several circular defects and numerous cracks originating from the sparking were observed on the surface. Figure 6b shows a high-magnification tiled SEM image of the flat region without any defect. A thin, uniform barrier oxide film with a thickness of approximately 400 nm on the was formed on the surface. It was experimentally reported that the thickness of the barrier layer, δ_{bb}, formed by anodizing can be calculated with the anodizing voltage, U_a, as follows [40-42]:

$$\delta_{bb} = kU_a \qquad (1)$$

where k is the proportionality constant of approximately 1.5 nmV^{-1}. The thickness of the barrier layer shown in Fig. 6b (approximately 400 nm) is in good agreement with the calculated value (378 nm at 252 V). On the other hand, a high-magnification SEM image of the circular defect exhibited a different morphology possessing a melted and then rapidly solidified microporous structure (Fig. 6c). Hill-like protrusions with micropores and crevices also appeared in the initial stage of sparking. Figure 6d shows an SEM image of the fractured cross section of the protuberant defect. Note that an AAO film with nanoscale pores was observed under the outer PEO film. Namely, localized sparking in the barrier oxide film leads to the formation of a characteristic multi-layer structure consisting of the outer PEO film and inner AAO film.

Figures 7a and 7b show SEM images of the fractured cross section of the specimen covered completely with the multi-layer anodic oxide film, which is formed by anodizing in a 2.0 M ammonium carbonate solution (333 K) for 180 min at a) 25 Am^{-2} and b) 50 Am^{-2}, respectively. Here, the specimens were bent 90 degrees downward to obtain the fractured cross-section of the anodic oxide. The multi-layer oxide structures were remained on the aluminum substrate after the bending of the specimens, and no visible peeling of the film was observed. Although several void defects were observed inside the inner AAO film, a PEO/AAO multi-layer anodic oxide film was

continuously formed on the whole aluminum substrate. High-magnification SEM images of the outer PEO layer and inner AAO layer formed at 50 Am^{-2} are shown in Figs. 7c and 7d, respectively. A typical PEO film possessing a microporous structure was observed on the surface (Fig. 7c) [43]. Additionally, a typical AAO film consisting of an outer nanoporous layer with vertical pores and an inner hemispherical barrier layer can be observed here (Fig. 7d). The thickness of the bottom barrier layer was measured to be approximately 340-410 nm, although the thickness strongly depends on the fracture positions. It was experimentally reported that the thickness of the barrier layer formed at the bottom AAO, δ_{bp}, by anodizing can be calculated using the anodizing voltage, U_a, as follows [44, 45]:

$$\delta_{bp} = kU_a \qquad (2)$$

where k is the proportionality constant of approximately 1.0-1.1 nmV^{-1}. Because the anodizing voltage under this operating condition was measured to be approximately 380 V, the thickness of the barrier layer can be calculated as 380-418 nm, in good agreement with the experimental value.

Based on these SEM observations described above, we would like to discuss the growth behavior of the PEO/AAO multi-layer structure formed by anodizing aluminum in ammonium carbonate solutions (Figure 8). The pH values of ammonium carbonate solution used in this investigation were measured to be 8.1-8.7. This weak alkaline solution may cause the formation of barrier oxide film and subsequent visible sparking behaviors at high voltages. In the initial stage of galvanostatic anodizing, the voltage linearly and rapidly increases with the anodizing time (Figs. 2 and 3) due to the growth of the uniform barrier oxide film on the aluminum substrate (Figs. 3 and 6). As the voltage reached the first plateau region, continuous visible sparking behaviors began in the barrier oxide film, and the circularly protuberant oxide was formed (Fig. 6). This anodic oxide consists of the multi-layer structure with the outer PEO film and inner AAO film. Why the AAO film is formed under the PEO film via the sparking is unclear but can be ascribed to the solubility of the anodic oxide. As the local temperature of the ammonium carbonate solution increases with sparking, the AAO film may be instantaneously formed under the microporous PEO film due to increasing solubility of the aluminum oxide. The withstanding voltage of the barrier layer formed under the AAO film was higher than that of the barrier oxide film formed in the initial stage. Therefore, the PEO/AAO multi-layer was gradually expanded by continuous sparking in the initial barrier oxide film, and then the aluminum specimen was completely covered with the PEO/AAO multi-layer (Fig. 3). Finally, the voltage increased with the anodizing time once again due to complete covering of the PEO/AAO multi-layer (Figs. 2 and 3), and the thickness of the PEO/AAO multi-layer increases with the anodizing time due to sparking in the multi-layer (Figs. 4 and 7).

In 2019, Huang et al. reported that Microarc oxidation (MAO)/AAO double layers could be formed by anodizing in etidronic acid [46,47]. Etidronic acid anodizing also operates at high voltages measuring more than 200 V. Thus, similar multi-layer

structure may grow via high-voltage anodizing in other electrolyte solution under appropriate operating conditions such as temperature and pH values.

Figure 9 shows the X-ray diffraction patterns obtained from the a) electropolished aluminum and b) specimen anodized at 50 Am^{-2} and 333 K for 180 min. Two strong peaks corresponding to metallic aluminum (200) and (220) were measured from the electropolished aluminum surface (Fig. 9a). Because the aluminum specimen was anodized to form the PEO/AAO multi-layer structure, the diffraction pattern associated with the metallic aluminum and crystalline γ-aluminum oxide was obtained from the specimen (Fig. 9b). Additionally, a small broad peak was evident corresponding to amorphous aluminum oxide at 10-40 degrees. It was been reported that typical anodizing aluminum in acidic or alkaline solutions leads to the formation of amorphous AAO film on the aluminum substrate [48,49]. Therefore, the multi-layer structure consisting of the outer PEO layer with crystalline γ-Al_2O_3 and the inner AAO layer with amorphous Al_2O_3 was formed on the aluminum surface by anodizing in ammonium carbonate.

The aluminum specimen covering the PEO/AAO multi-layer structure was immersed in boiling ultrapure water for 15 min to seal the pores. Figure 10 shows SEM images of a) the surface of the PEO film and b) fractured cross section of AAO film after immersion. Nanoscale numerous plate-like hydroxides were formed on the whole surface of the PEO film by the hydration of anodic oxide as follows (Fig. 10a) [50]:

$$Al_2O_3 + H_2O \rightarrow 2AlO(OH) \qquad (3)$$

Similarly, the inner AAO film was also hydrated after immersion in boiling water, and the nanopores formed in the AAO film was completely filled with the hydroxide (pore-sealing, Fig. 10b). Therefore, it is expected that the pore-sealed PEO/AAO multi-layer structure fabricated by anodizing in ammonium carbonate and subsequent pore-sealing may be useful for the corrosion-resistant PEO/AAO coating process of various aluminum alloys. Further investigations by anodizing of various aluminum alloys in ammonium carbonate and subsequent analysis for the corrosion protection and mechanical strength are required near future.

4. Conclusions

The growth behavior of anodic oxide films formed via the galvanostatic anodizing of aluminum in alkaline ammonium carbonate solution was investigated by electrochemical measurement and electron microscopy. An uneven surface with a nonuniform dark gray oxide film was formed by anodizing in a lower concentration of 0.3 M ammonium carbonate solution. Characteristic voltage-time curves with two high-plateau voltages at approximately 250 V and 375 V were obtained during anodizing aluminum in a higher concentration of 2.0 M ammonium carbonate solution, and a uniform oxide film with a light gray hue was formed on the surface by anodizing at a higher temperature of 333 K. This anodizing condition led to the formation of a uniform PEO/AAO multi-layer structure on the aluminum substrate through the barrier

layer formation and subsequent continuous visible sparking. The multi-layer structure consisted of an outer PEO film with crystalline γ-Al_2O_3 and inner AAO film with amorphous Al_2O_3. The average thickness of the multi-layer oxide film increased with the anodizing time, although the growth rate gradually decreased. The nanopores formed in the AAO film can be filled with hydroxides via subsequent immersion in boiling water.

Acknowledgments

We would like to thank Mr. Nobuyuki Miyazaki and Dr. Takashi Endo for their assistance in the SEM observations. This investigation was supported in part by the Japan Society for the Promotion of Science (JSPS) KAKENHI, Japan, the Light Metal Education Foundation, Japan, and the Fundamental Research Developing Association for Shipbuilding and Offshore, Japan.

References

1) G.E. Thompson, Porous anodic alumina: fabrication, characterization and applications, Thin Solid Films 297 (1997) 192-201.
2) W. Lee, D. J. Park, Porous anodic aluminum oxide: anodization and templated synthesis of functional nanostructures, Chem. Rev. 114 (2014) 7487-7556.
3) G.D. Sulka, Highly ordered anodic porous alumina formation by self-organized anodizing, Chap. 1 in: A. Eftekhari (Ed.), Nanostructured Materials in Electrochemistry, Wiley-VCH, 2008, pp. 1-116. doi:10.1002/9783527621507.ch1
4) T. Kudo, R.S. Alwitt, Cross-sections of hydrous and composite aluminum oxide films, Electrochim. Acta 23 (1978) 341-345.
5) K. Shimizu, G.E. Thompson, G.C. Wood, Direct observation of the duplex nature of anodic barrier films on aluminum, Thin Solid Films 81 (1981) 39-44.
6) H. Habazaki, K. Shimizu, P. Skeldon, G.E. Thompson, G.C. Wood, The incorporation of metal ions into anodic films on aluminium alloys, Philos. Mag. B 73 (1996) 445-460.
7) K. Shimizu, G.E. Thompson, G.C. Wood, Electron-beam-induced crystallization of anodic barrier films on aluminium, Thin Solid Films 77 (1981) 313-318.
8) K. Watanabe, M. Sakairi, H. Takahashi, K. Takahiro, S. Nagata, S. Hirai, Anodizing of aluminum coated with silicon oxide by a sol-gel method, J. Electrochem. Soc. 148 (2001) B473-B481.
9) G.D. Sulka, S. Stroobants, V. Moshchalkov, G. Borghs, J.P. Celis, Synthesis of well-ordered nanopores by anodizing aluminum foils in sulfuric acid, J. Electrochem. Soc. 149 (2002) D97-D103.
10) S. Akiya, T. Kikuchi, S. Natsui, R.O. Suzuki, Optimum exploration for the self-ordering of anodic porous alumina formed via selenic acid anodizing, J. Electrochem. Soc. 162 (2015) E244-E250.
11) G.D. Sulka, W.J. Stępniowski, Structural features of self-organized nanopore arrays

formed by anodization of aluminum in oxalic acid at relatively high temperatures, Electrochim. Acta 54 (2009) 3683-3691.
12) S. Akiya, T. Kikuchi, S. Natsui, N. Sakaguchi, R.O. Suzuki, Self-ordered porous alumina fabricated via phosphonic acid anodizing, Electrochim. Acta 190 (2016) 471-479.
13) H. Masuda, K. Yada, A. Osaka, Self-ordering of cell configuration of anodic porous alumina with large-size pores in phosphoric acid solution, Jpn. J. Appl. Phys. 37 (1998) L1340.
14) T. Kikuchi, O. Nishinaga, S. Natsui, R.O. Suzuki, Fabrication of self-ordered porous alumina via etidronic acid anodizing and structural color generation from submicrometer-scale dimple array, Electrochim. Acta 156 (2015) 235-243.
15) T. Kikuchi, K. Kunimoto, H. Ikeda, D. Nakajima, R.O. Suzuki, S. Natsui, Fabrication of anodic porous alumina via galvanostatic anodizing in alkaline sodium tetraborate solution and their morphology, J. Electroanal. Chem. 846 (2019) 113152.
16) T.P. Hoar, G.C. Wood, The sealing of porous anodic oxide films on aluminium, Electrochim. Acta 7 (1962) 333-353.
17) Y. Suzuki, K. Kawahara, T. Kikuchi, R.O. Suzuki, S. Natsui, Corrosion-Resistant Porous Alumina Formed via Anodizing Aluminum in Etidronic Acid and Its Pore-Sealing Behavior in Boiling Water, J. Electrochem. Soc. 166 (2019) C261-C269.
18) T. He, Y. Wang, Y. Zhang, T. Xu, T. Liu, Super-hydrophobic surface treatment as corrosion protection for aluminum in seawater, Corr. Sci. 51 (2009) 1757-1761.
19) V.R. Capelossi, M. Poelman, I. Recloux, R.P.B. Hernandez, H.G. De Melo, M.G. Olivier, Corrosion protection of clad 2024 aluminum alloy anodized in tartaric-sulfuric acid bath and protected with hybrid sol–gel coating, Electrochim. Acta 124 (2014) 69-79.
20) T. Kikuchi, Y. Hara, M. Sakairi, T. Yonezawa, A. Yamauchi, H. Takahashi, Corrosion of Al–Sn–Bi alloys in alcohols at high temperatures. Part II: Effect of anodizing on corrosion, Corr. Sci. 52 (2010) 2525-2534.
21) L. Wen, R. Xu, Y. Mi, Y. Lei, Multiple nanostructures based on anodized aluminium oxide templates, Nat. Nanotechnol. 12 (2017) 244-252.
22) T. Ozel, G.R. Bourret, C.A. Mirkin, Coaxial lithography Nat. Nanotechnol. 10 (2015) 319-324.
23) T. Yanagishita, K. Nishio, H. Masuda, Anti-reflection structures on lenses by nanoimprinting using ordered anodic porous alumina, Appl. Phys. Express 2 (2009) 022001.
24) T. Kondo, K. Nishio, H. Masuda, Surface-enhanced Raman scattering in multilayered Au nanoparticles in anodic porous alumina matrix, Appl. Phys. Express 2 (2009) 032001.
25) T. Kikuchi, O. Nishinaga, S. Natsui, R.O. Suzuki, Polymer nanoimprinting using an anodized aluminum mold for structural coloration, Appl. Surf. Sci. 341 (2015) 19-27.

26) D. Nakajima, T. Kikuchi, S. Natsui, R.O. Suzuki, Advancing and receding contact angle investigations for highly sticky and slippery aluminum surfaces fabricated from nanostructured anodic oxide, RSC Adv. 8 (2018) 37315-37323.
27) R.O. Hussein, X. Nie, D.O. Northwood, A. Yerokhin, A. Matthews, Spectroscopic study of electrolytic plasma and discharging behaviour during the plasma electrolytic oxidation (PEO) process, J. Phys. D 43 (2010) 105203.
28) G. Wei-Chao, L. Guo-Hua, C. Huan, C. Guang-Liang, F. Wen-Ran, Z. Gu-Ling, Y. Si-Ze, Investigation of morphology and composition of plasma electrolytic oxidation coatings in systems of Na_2SiO_3–NaOH and $(NaPO_3)_6$–NaOH, J. Mater. Process. Technol. 182 (2007) 28-33.
29) S. Moon, Y. Jeong, Generation mechanism of microdischarges during plasma electrolytic oxidation of Al in aqueous solutions, Corr. Sci. 51 (2009) 1506-1512.
30) S. Moon, Y. Kim, Lateral growth of PEO films on Al1050 alloy in an alkaline electrolyte, J. Korean Inst. Surf. Eng. 50 (2017) 10-16.
31) A. Nominé, J. Martin, C. Noël, G. Henrion, T. Belmonte, I.V. Bardin, P. Lukeš, Surface charge at the oxide/electrolyte interface: toward optimization of electrolyte composition for treatment of aluminum and magnesium by plasma electrolytic oxidation, Langmuir 32 (2016) 1405-1409.
32) D.A. Becerik, A. Ayday, L.C. Kumruoğlu, S.C. Kurnaz, A. Özel, The effects of Na_2SiO_3 concentration on the properties of plasma electrolytic oxidation coatings on 6060 aluminum alloy, J. Mater. Eng. Perform. 21 (2012) 1426-1430.
33) Q.P. Tran, T.S. Chin, Y.C. Kuo, C.X. Jin, T. Trung, C. Van Tuan, D.Q. Dang, Diamond powder incorporated oxide layers formed on 6061 Al alloy by plasma electrolytic oxidation, J. Alloys Compd. 751 (2018) 289-298.
34) S. Stojadinovic, R. Vasilic, I. Belca, M. Petkovic, B. Kasalica, Z. Nedic, L. Zekovic, Characterization of the plasma electrolytic oxidation of aluminium in sodium tungstate, Corr. Sci. 52 (2010) 3258-3265.
35) H.X. Li, V.S. Rudnev, X.H. Zheng, T.P. Yarovaya, R.G. Song, Characterization of Al_2O_3 ceramic coatings on 6063 aluminum alloy prepared in borate electrolytes by micro-arc oxidation, J. Alloys Compd. 462 (2008) 99-102.
36) Y.J. Oh, J.I. Mun, J.H. Kim, Effects of alloying elements on microstructure and protective properties of Al_2O_3 coatings formed on aluminum alloy substrates by plasma electrolysis, Surf. Coat. Technol. 204 (2009) 141-148.
37) J.M. Wheeler, J.A. Curran, S. Shrestha, Microstructure and multi-scale mechanical behavior of hard anodized and plasma electrolytic oxidation (PEO) coatings on aluminum alloy 5052, Surf. Coat. Technol. 207 (2012) 480-488.
38) U. Malayoglu, K.C. Tekin, U. Malayoglu, S. Shrestha, An investigation into the mechanical and tribological properties of plasma electrolytic oxidation and hard-anodized coatings on 6082 aluminum alloy, Mater. Sci. Eng. A 528 (2011) 7451-7460.
39) T. Kikuchi, M. Sakairi, H. Takahashi, Three-dimensional microstructure fabrication

with aluminum anodizing, laser irradiation, and electrodeposition, J. Electrochem. Soc. 150 (2003) C567-C572.
40) R.C. McCune, H.K. Plummer, Transmission electron microscopy of ultramicrotomed barrier anodic films on aluminium, Surf. Interface Anal. 4 (1982) 257-260.
41) H. Asoh, K. Uchibori, S. Ono, Structural features of anodic oxide films formed on aluminum substrate coated with self-assembled microspheres, Corr. Sci. 51(2009) 1496-1500.
42) H. Takahashi, K. Fujimoto, H. Konno, M. Nagayama, Distribution of anions and protons in oxide films formed anodically on aluminum in a phosphate solution, J. Electrochem. Soc. 131 (1984) 1856-1861.
43) M. Mohedano, E. Matykina, R. Arrabal, B. Mingo, A. Pardo, PEO of pre-anodized Al–Si alloys: Corrosion properties and influence of sealings, Appl. Surf. Sci. 346 (2015) 57-67.
44) I. Vrublevsky, V. Parkoun, J. Schreckenbach, Analysis of porous oxide film growth on aluminum in phosphoric acid using re-anodizing technique, Appl. Surf. Sci. 242 (2005) 333-338.
45) S.Z. Chu, K. Wada, S. Inoue, M. Isogai, Y. Katsuta, A. Yasumori, Large-scale fabrication of ordered nanoporous alumina films with arbitrary pore intervals by critical-potential anodization, J. Electrochem. Soc. 153 (2006) B384-B391.
46) H. Huang, J. Qiu, M. Sun, W. Liu, X. Wei, E. Sakai, K. Ito, A hard coating with MAO/AAO double layers prepared on aluminum in etidronic acid by DC oxidation, Surf. Coat. Technol. 360 (2019) 307-317.
47) H. Huang, J. Qiu, M. Sun, W. Liu, X. Wei, Morphological evolution and burning behavior of oxide coating fabricated on aluminum immersed in etidronic acid at high current density, Surf. Coat. Technol. 374 (2019) 83-94.
48) A. Takenaga, T. Kikuchi, S. Natsui, R.O. Suzuki, Exploration for the self-ordering of porous alumina fabricated via anodizing in etidronic acid, Electrochim. Acta 211 (2016) 515-523.
49) S. Akiya, T. Kikuchi, S. Natsui, R.O. Suzuki, Nanostructural characterization of large-scale porous alumina fabricated via anodizing in arsenic acid solution, Appl. Surf. Sci. 403 (2017) 652-661.
50) Y. Suzuki, K. Kawahara, T. Kikuchi, R.O. Suzuki, S. Natsui, Corrosion-Resistant Porous Alumina Formed via Anodizing Aluminum in Etidronic Acid and Its Pore-Sealing Behavior in Boiling Water, J. Electrochem. Soc. 166 (2019) C261-C269.

Figure Captions

Figure 1 Changes in the voltage, U_a, with time, t_a, during anodizing aluminum in a 0.3 M ammonium carbonate solution (333K) at 25-200 Am^{-2} for 120 min. An inset photo shows the surface appearance of the aluminum specimen anodized at 50 Am^{-2} for 120 min.

Figure 2 Voltage-time curves obtained via anodizing aluminum in a 2.0 M ammonium carbonate solution at a) 283 K, b) 303 K, and c) 333 K and 25-400 Am^{-2} for 120 min. The surface appearances of the specimen anodized at 50 Am^{-2} for 120 min are shown in each figure.

Figure 3 a) Voltage-time curve obtained via anodizing aluminum in a 2.0 M ammonium carbonate solution (333 K) at 25 Am^{-2} for 300 min. b), c) SEM images of the b) surface and c) vertical cross section of the specimen anodized for 3-300 min. d) A high-magnification SEM image of the specimen anodized for 180 min.

Figure 4 Changes in the thickness of the oxide film, δ, with anodizing time, t_a, obtained via anodizing in a 2.0 M ammonium carbonate solution (333 K) at a) 25 Am^{-2} and b) 50 Am^{-2} for up to 670 min.

Figure 5 SEM images of the vertical cross section of the specimen anodized in a 2.0 M ammonium carbonate solution (333 K) at 25 Am^{-2} for 670 min a) before and b) after chemical etching in a NaOH/ $K_3[Fe(CN)_6]$ solution.

Figure 6 a) An SEM image of the surface of the specimen anodized in a 2.0 M ammonium carbonate solution (333 K) at 25 Am^{-2} for 10 min. b) A tiled SEM image of the fractured cross section of the barrier oxide film. c) A tiled SEM image of the surface of the plasma electrolytic oxidation (PEO) film. d) A high-magnification SEM image of the fractured cross section of the PEO/anodic aluminum oxide (AAO) multi-layer structure.

Figure 7 a), b) Tiled SEM images of the fractured cross section of the PEO/AAO multi-layer structure obtained via anodizing in a 2.0 M ammonium carbonate solution (333 K) for 180 min at a) 25 Am^{-2} and b) 50 Am^{-2}, respectively. c), d) High-magnification SEM images of the fractured cross section of the c) outer PEO film and d) inner AAO film formed at 50 Am^{-2}, respectively.

Figure 8 Schematic model illustrating the formation behavior of the PEO/AAO multi-layer structure via anodizing in ammonium carbonate.

Figure 9 X-ray diffraction patterns of the a) electropolished aluminum and b) aluminum anodized in a 2.0 M ammonium carbonate solution (333 K) at 50 Am^{-2} for 180 min.

Figure 10 SEM images of a) the surface of the PEO film and b) fractured cross section of the AAO film after immersion in boiling ultrapure water for 15 min.

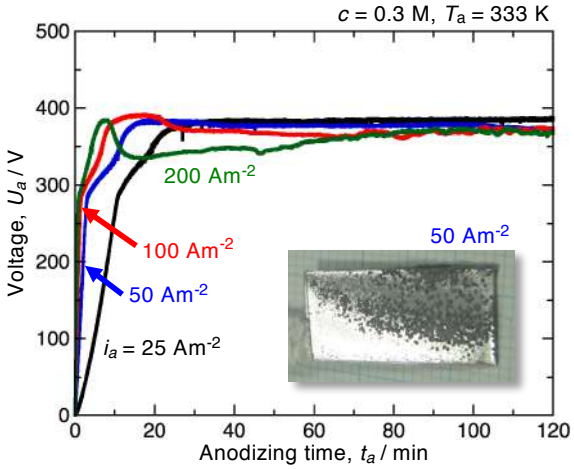
c = 0.3 M, T_a = 333 K
500
400
300
200
100
0
Voltage, U_a / V
0
20
40
60
80
100
120
Anodizing time, t_a / min
200 Am-2
100 Am-2
50 Am-2
i_a = 25 Am-2
50 Am-2

Figure 1.

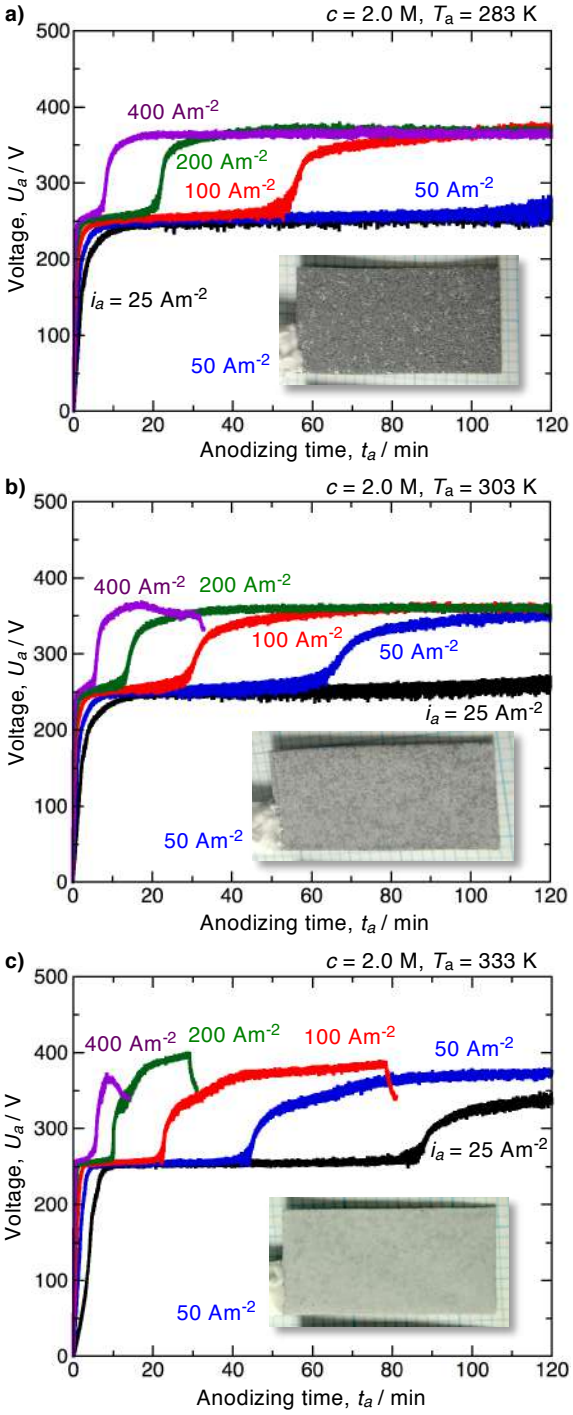
a)
c = 2.0 M, Ta = 283 K
400 Am-2
200 Am-2
100 Am-2
50 Am-2
ia = 25 Am-2
50 Am-2
Voltage, Ua / V
Anodizing time, ta / min
b)
c = 2.0 M, Ta = 303 K
400 Am-2
200 Am-2
100 Am-2
50 Am-2
ia = 25 Am-2
50 Am-2
Voltage, Ua / V
Anodizing time, ta / min
c)
c = 2.0 M, Ta = 333 K
400 Am-2
200 Am-2
100 Am-2
50 Am-2
ia = 25 Am-2
50 Am-2
Voltage, Ua / V
Anodizing time, ta / min

Figure 2.

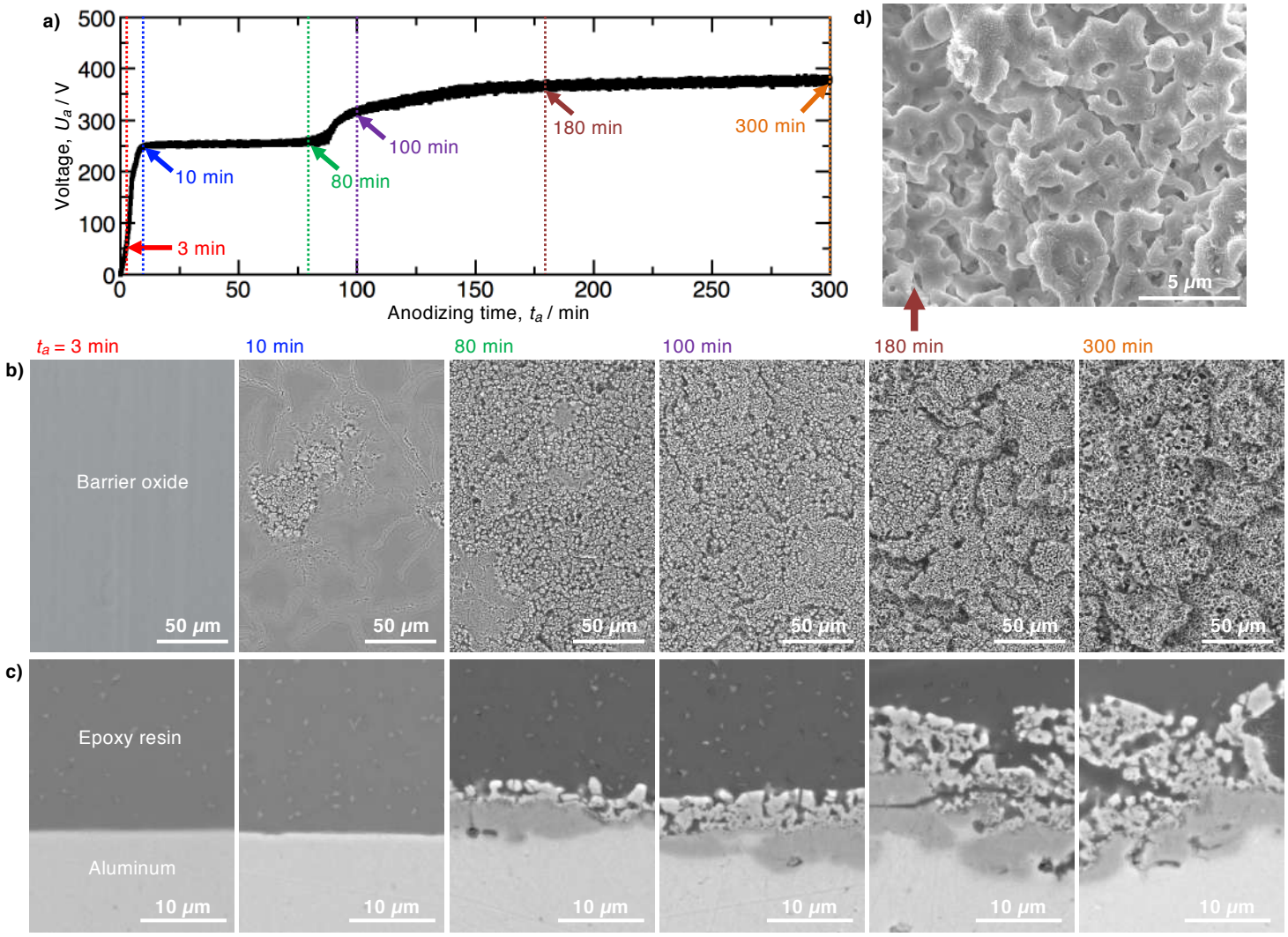
a)
Voltage, U_a / V
Anodizing time, t_a / min
3 min
10 min
80 min
100 min
180 min
300 min
d)
5 μm
t_a = 3 min
10 min
80 min
100 min
180 min
300 min
b)
Barrier oxide
50 μm
c)
Epoxy resin
Aluminum
10 μm

Figure 3.

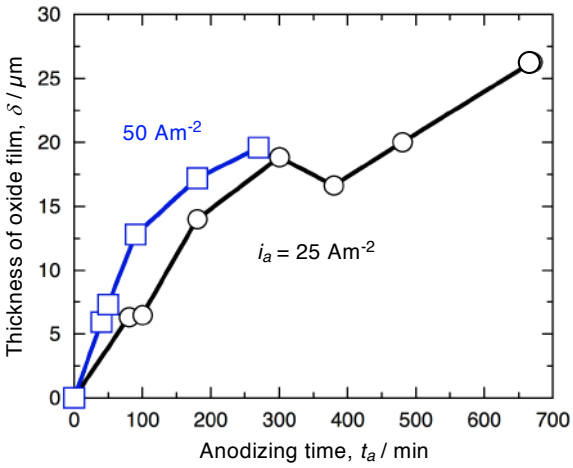
30
25
20
15
10
5
0
0
100
200
300
400
500
600
700
Thickness of oxide film, δ / μm
Anodizing time, t_a / min
50 Am^{-2}
i_a = 25 Am^{-2}

Figure 4.

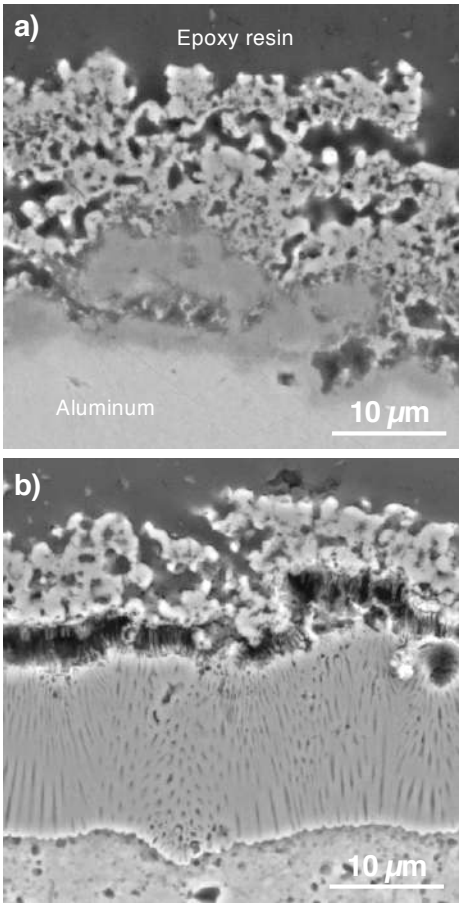

Figure 5.

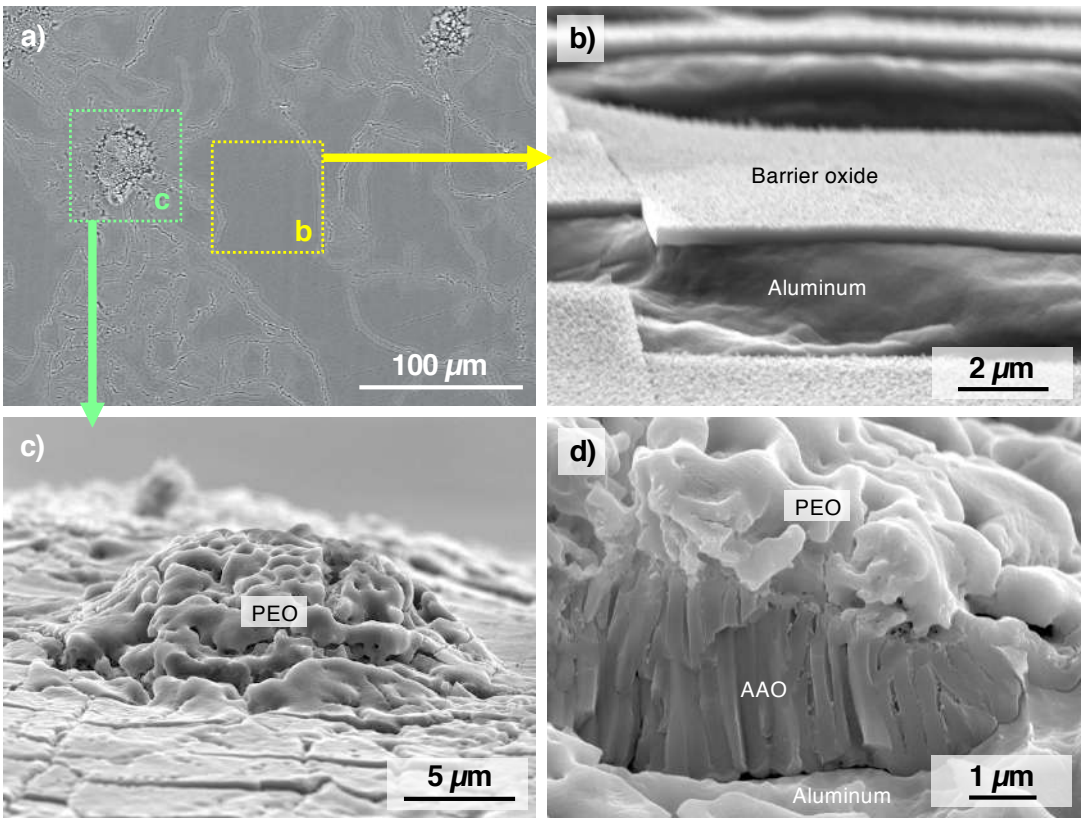
a)
c
b
100 μm
b)
Barrier oxide
Aluminum
2 μm
c)
PEO
5 μm
d)
PEO
AAO
Aluminum
1 μm

Figure 6.

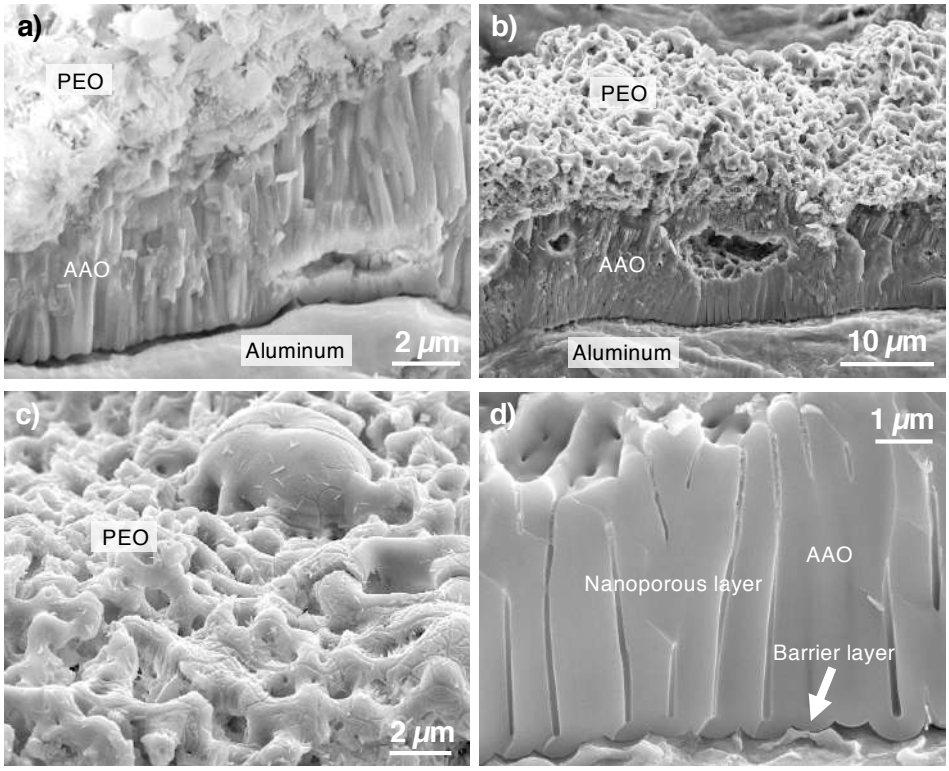
a)
PEO
AAO
Aluminum
2 μm
b)
PEO
AAO
Aluminum
10 μm
c)
PEO
2 μm
d)
1 μm
AAO
Nanoporous layer
Barrier layer

Figure 7.

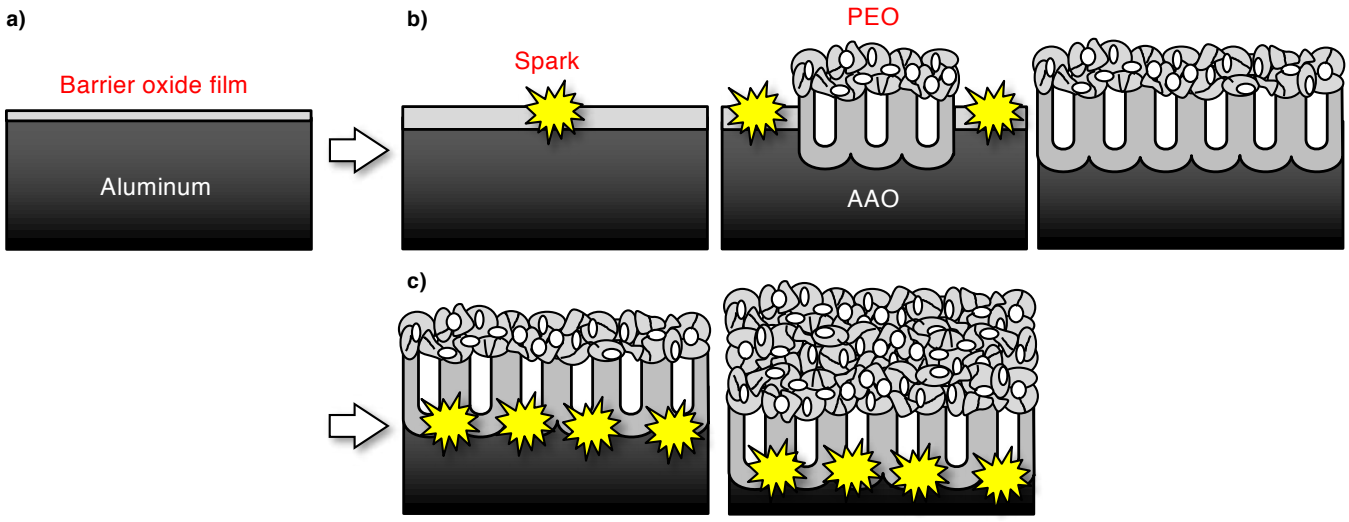

Figure 8.

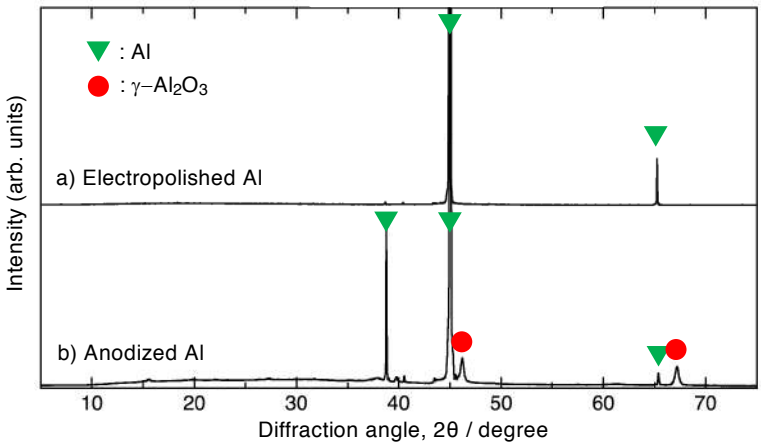
: Al
: γ–Al2O3
a) Electropolished Al
b) Anodized Al
Intensity (arb. units)
10
20
30
40
50
60
70
Diffraction angle, 2θ / degree

Figure 9.

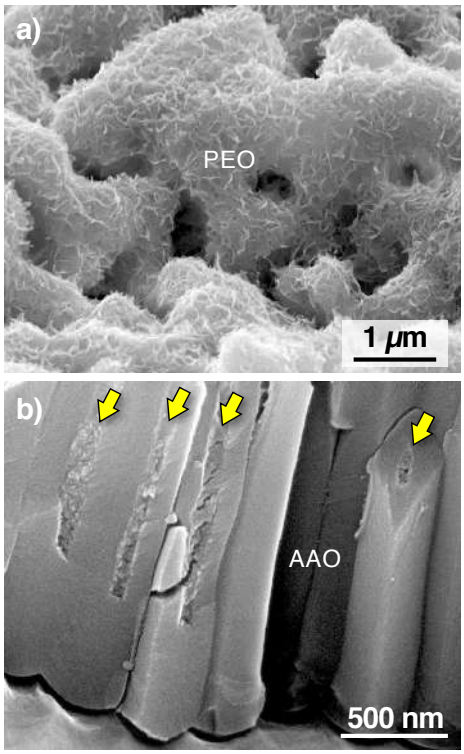

Figure 10.